Systems/Circuits

NMDA-Dependent Phase Synchronization between Septal and Temporal CA3 Hippocampal Networks

Ning Gu,* Jesse Jackson,* Romain Goutagny, Germaine Lowe, Frédéric Manseau, and Sylvain Williams
McGill University, Douglas Mental Health University Institute, Montreal, Quebec H4H 1R3, Canada

Increasing evidence suggests that synchronization between brain regions is essential for information exchange and memory processes. However, it remains incompletely known which synaptic mechanisms contribute to the process of synchronization. Here, we investigated whether NMDA receptor-mediated synaptic plasticity was an important player in synchronization between septal and temporal CA3 areas of the rat hippocampus. We found that both the septal and temporal CA3 regions intrinsically generate weakly synchronized δ frequency oscillations in the complete hippocampus *in vitro*. Septal and temporal oscillators differed in frequency, power, and rhythmicity, but both required $GABA_A$ and AMPA receptors. NMDA receptor activation, and most particularly the NR2B subunit, contributed considerably more to rhythm generation at the temporal than the septal region. Brief activation of NMDA receptors by application of extracellular calcium dramatically potentiated the septal–temporal coherence for long durations (>40 min), an effect blocked by the NMDA antagonist AP-5. This long-lasting NMDA-receptor-dependent increase in coherence was also associated with an elevated phase locking of spikes locally and across regions. Changes in coherence between oscillators were associated with increases in phase locking between oscillators independent of oscillator amplitude. Finally, although the septal CA3 rhythm preceded the oscillations in temporal regions in control conditions, this was reversed during the NMDA-dependent enhancement in coherence, suggesting that NMDA receptor activation can change the direction of information flow along the septotemporal CA3 axis. These data demonstrate that plastic changes in communication between septal and temporal hippocampal regions can arise from the NMDA-dependent phase locking of neural oscillators.

Introduction

The hippocampus is responsible for processing both spatial memory and emotion-related behavior, and increasing evidence suggests that these functions are segregated anatomically in the septal and temporal regions, respectively (Swanson and Cowan, 1977; Moser and Moser, 1998; Moser et al., 1993; Fanselow and Dong, 2010). This segregation in function results from a number of factors, such as the distinct input and output of each region, the local connectivity patterns, and the different molecular constituents of the local circuitry (Swanson and Cowan, 1977; Fanselow and Dong, 2010). Such segregation has also been demonstrated physiologically as the septal and temporal CA3 regions can generate θ rhythms that are weakly synchronized (Royer et al., 2010; Adhikari et al., 2011). There is also evidence that under certain laboratory paradigms, such as in fear conditioning, both the septal and temporal areas are necessary (Bast et al., 2009), whereas others have suggested that the intermediate hippocampus could be an integrative zone for different sensory modalities gathered by both hippocampal poles (Steffenach et al., 2002).

It is clear that communication between brain areas involves phase synchronization of oscillations (Rodriguez et al., 1999; Fries, 2005; Palva et al., 2005). Because the phase of the oscillation determines exactly when assemblies of neurons spike, it has been postulated that two brain areas with increased phase synchrony will have enhanced synaptic interaction and information exchange (Fell and Axmacher, 2011). An increase in spike timing precision between different regions resulting from enhanced phase locking may also promote plasticity of the synaptic connections, leading to long-term potentiation and memory formation. Enhancements in phase synchrony in the θ frequency range (~4–8 Hz) between the hippocampus and the prefrontal cortex have been shown to be associated with the quality of behavioral performance in working memory tasks (Benchenane et al., 2010; Sigurdsson et al., 2010; Adhikari et al., 2011; Fujisawa and Buzsáki, 2011). Similarly, a robust enhancement of spectral coherence at θ frequency between the amygdala and hippocampus occurs in fear memory retrieval (Seidenbecher et al., 2003; Popa et al., 2010) or between the lateral entorhinal cortex and PFC during associative learning (Takehara-Nishiuchi et al., 2011). In mice with genetic knockdown of NMDA receptor function, impaired phase synchrony is observed between the hippocampus

Received Jan. 9, 2013; revised March 29, 2013; accepted April 3, 2013.

Author contributions: N.G., J.J., and S.W. designed research; N.G., R.G., G.L., and F.M. performed research; J.J. contributed unpublished reagents/analytic tools; N.G. and J.J. analyzed data; N.G., J.J., and S.W. wrote the paper.

This work was supported by the Canadian Institutes of Health Research and the Natural Sciences and Engineering Research Council of Canada. N.G. was supported by a fellowship from Fonds de la Recherche en Santé du Québec. R.G. was supported by the Conrad F. Harrington postdoctoral fellowship from the McGill Faculty of Medicine. J.J. received a Canadian Graduate Scholarship from Natural Sciences and Engineering Research Council of Canada and an Ann & Richard Sievers Award.

The authors declare no competing financial interests.

*N.G. and J.J. contributed equally to this work.

Correspondence should be addressed to Dr. Sylvain Williams, Department of Psychiatry, McGill University, Douglas Mental Health University Institute, 6875 Lasalle Boulevard, Verdun, Quebec H4H 1R3, Canada. E-mail: sylvain.williams@gmail.com.

DOI:10.1523/JNEUROSCI.0179-13.2013

 0270-6474/13/338276-12$15.00/0

and cortex (Dzirasa et al., 2009). Despite the evidence that increases in neural synchrony are associated with different forms of memory processes, direct evidence showing that increased phase coherence can underlie plasticity related changes is still lacking at the cellular level.

The general aim of this study was to determine whether increases in phase synchrony between two regions is dependent on NMDA receptor and plasticity-dependent mechanisms. Our results suggest that NMDA receptors play a significant role in the long-term potentiation of spectral coherence between hippocampal areas through phase–phase synchrony and may be involved in long-term changes in coherence observed during different memory tasks *in vivo*. Portions of these results were presented at the Society for Neuroscience annual meeting in 2011 (Gu et al., 2011).

Materials and Methods

Dissection. All procedures were performed according to protocols and guidelines approved by the McGill University Animal Care Committee and the Canadian Council on Animal Care. Male and female Sprague Dawley rats (P15–P22) were decapitated, and the brain was rapidly removed from the skull and placed in ice-cold high sucrose artificial CSF (aCSF) solution (in mM: 252 sucrose, 3 KCl, 2 $MgSO_4$ 24 NaHCO3, 1.25 NaH_2PO_4, 1.2 CaCl2, and 10 glucose) and bubbled with carbogen (95% O_2 and 5% CO_2). The cerebellum and frontal cortex were removed with a razor blade, and the two hemispheres were separated and allowed to recover for 2–3 min in the oxygenated sucrose solution. The single hippocampal isolate was then removed from the remaining hemisection in the manner described previously (Goutagny et al., 2009). The entire hippocampal isolation procedure was completed within 1 min. After dissection, the hippocampal complex was left at room temperature in aCSF bubbled with carbogen for 60–180 min. For recording, the preparation was transferred quickly to a custom-made submerged recording chamber. Recordings were performed at 30°C-32°C after an additional 30 min period in the chamber.

In the experiments where CA1 and dentate gyrus (DG) were removed (the longitudinal cut), a thin razor blade was placed through the septotemporal extent of the entire hippocampus at an angle to disconnect the CA3-CA1 pathway and at the same time separate the DG from CA3. This procedure also removed the most extreme septal and temporal ends of CA1. To ensure that the CA1 and DG were removed from CA3, after the completion of the experiment, the strip of isolated CA3 was fixed, sliced, and stained by using histology methods described below.

Recordings. The preparation was continuously perfused with aCSF (25 ml/min, in mM: 126 NaCl, 24 $NaHCO_3$, 10 glucose, 4.5 KCl, 2 $MgSO_4$, 1.25 NaH_2PO_4, and 2 $CaCl_2$, pH 7.4, with 95% O_2/5% CO_2) via a gravity-fed perfusion system and maintained at 30°C-32°C. Local field potentials were recorded using glass micropipettes (1–4 MΩ) filled with aCSF. Signals were recorded through a differential AC amplifier (A-M Systems), filtered online (0.1–500 Hz), and sampled at 5 KHz. Signals were referenced to the bath medium and connected to ground.

Data analysis. Electrophysiological data were digitized, analyzed, and plotted using pClamp, MATLAB, and Origin (version 7.5; OriginLab). Spectrograms were constructed using the Chronux tool box (Bokil et al., 2010), using a time frequency bandwidth of 2 with 3 tapers. The power and dominant frequency of the oscillation in the different CA3 locations were measured by taking the peak of the mean spectrogram from at least 5 min of continuous data. The oscillation strength was calculated by detecting the peak of the power spectrum of the autocorrelation function (using autocorrelation lags from −2 to +2 s).

The phase locking value (PLV) between pairs of local field potential (LFP) recordings was calculated using an approach similar to that described previously (Lachaux et al., 1999). The PLV between septal and temporal regions was quantified using at least 2 min of continuous data. First, the LFPs from both oscillators were bandpass filtered (0.5–5 Hz). The phase φ_{septal} and $\varphi_{temporal}$ of these filtered signals were then determined using the Hilbert transform in MATLAB (MathWorks). The phase difference between these two signals was then calculated ($\varphi_{diff} = \varphi_{septal} - \varphi_{temporal}$). This phase difference signal was then wrapped on the unit circle (from −180 to 180 degrees). If the two oscillators are phase shifted by a constant value, then the difference between phases will be constant at every time point. If there is no relationship between phases (oscillators are not phase synchronized), then this phase difference will drift and with enough data points will approach a uniform distribution. We calculated the mean resultant length (CircStat, toolbox) (Berens, 2009) of the phase difference vector, which yields a value between 0 and 1. This value is henceforth termed the PLV. A value of 1 indicates perfect phase synchrony (a constant phase difference between two signals), whereas a value of 0 indicates that the phase difference distribution is uniform.

To test the significance of the PLV, we generated a surrogate set of 200–400 PLVs by shuffling the data between 2 s and the length of the entire signal used for the original analysis (2–5 min). This procedure removes the temporal correlation between two signals while ensuring the statistical properties of the observed and shuffled dataset are not different. The original PLV was required to be greater than the mean ± 2 SD of this surrogate shuffled dataset to be considered statistically significant. For data expressing the PLV as a function of time, the PLV was analyzed in 10 s periods and moved sequentially through the data. For visualization, three consecutive PLV values were averaged together to display the mean PLV within each 30 s period. We also assessed the time lag at which the two oscillators were most synchronized. In this isolated hippocampal preparation, the two oscillators are thought to be communicating via synaptic connections, which would introduce a delay between a sender and receiver oscillator. For the analysis of PLV as a function of time lags (τ) between the oscillators, the septal oscillator was shifted in both the negative and positive direction ($\tau = -1$ to $+1$ s in 5 ms increments, PLV-shift) to observe the time lag of maximal phase locking. The septal oscillator was shifted in time using the circshift function in MATLAB. If the maximum PLV occurred at negative time lags, then this indicates that the septal oscillator is most synchronized with the recent history of the temporal oscillator and suggests that the temporal oscillator is influencing the septal oscillator after a delay. Similar shifting methods have previously been used to assess the time lag between spike–LFP synchrony (Siapas et al., 2005; Hangya et al., 2009). If the maximal PLV occurs at positive time lags, then the septal oscillator can be said to influence the temporal oscillator. These oscillators are independent and likely bidirectionally coupled; therefore, it should not be stated that one oscillator is "driving" or "pacing" the other oscillator.

The phase locking between spikes (single-unit or multiunit activity) and the LFP phase was determined using the entropy of the spike–LFP phase locking probability distribution. Because the LFPs recorded had large asymmetries, their phase values, as calculated with the Hilbert transform, are nonuniformly distributed from −180° to 180°. Therefore, even randomly generated spike trains will give the appearance of being phase-locked to the LFP unless some sort of correction is applied. Furthermore, using traditional circular statistics, such as the Rayleigh test, is not informative as we are not interested in testing whether a spike-phase probability distribution is different from uniformity, but rather from an empirically measured distribution that is determined by the phase distribution of the LFP. Therefore, rather than testing whether an observed distribution of spike phases (p) is different from uniform, we must test whether this distribution is different from phase distribution of LFP phases (q). In the case of a pure sine wave q is uniform, but in the case of most LFPs, uniformity is not observed. Therefore, we calculated the Kullback–Leibler divergence (D_{kl}) between the distributions p and q as follows: $D_{kl}\Sigma_{j=1}^{N} p_j \log\left[\frac{p_j}{q_j}\right]$. Where $N = 36$ (10°), phase bins and p_j and q_j are values of the probability distribution (p and q) in phase bins j. D_{kl} assumes a value ≥ 0 where 0 would indicate that the two distributions are equal. This difference is normalized by entropy of the distribution of q as follows: $H_q = -\Sigma_{j=1}^{N} q_j \log q_j$. The normalized measure of spike phase modulation is then expressed as $MI = D_{kl}/H_q$, where MI indicates modulation index. This normalized measure assumes a value between 0 and 1, where greater values indicate a greater divergence between the observed spike phase distribution and the distribution expected with random

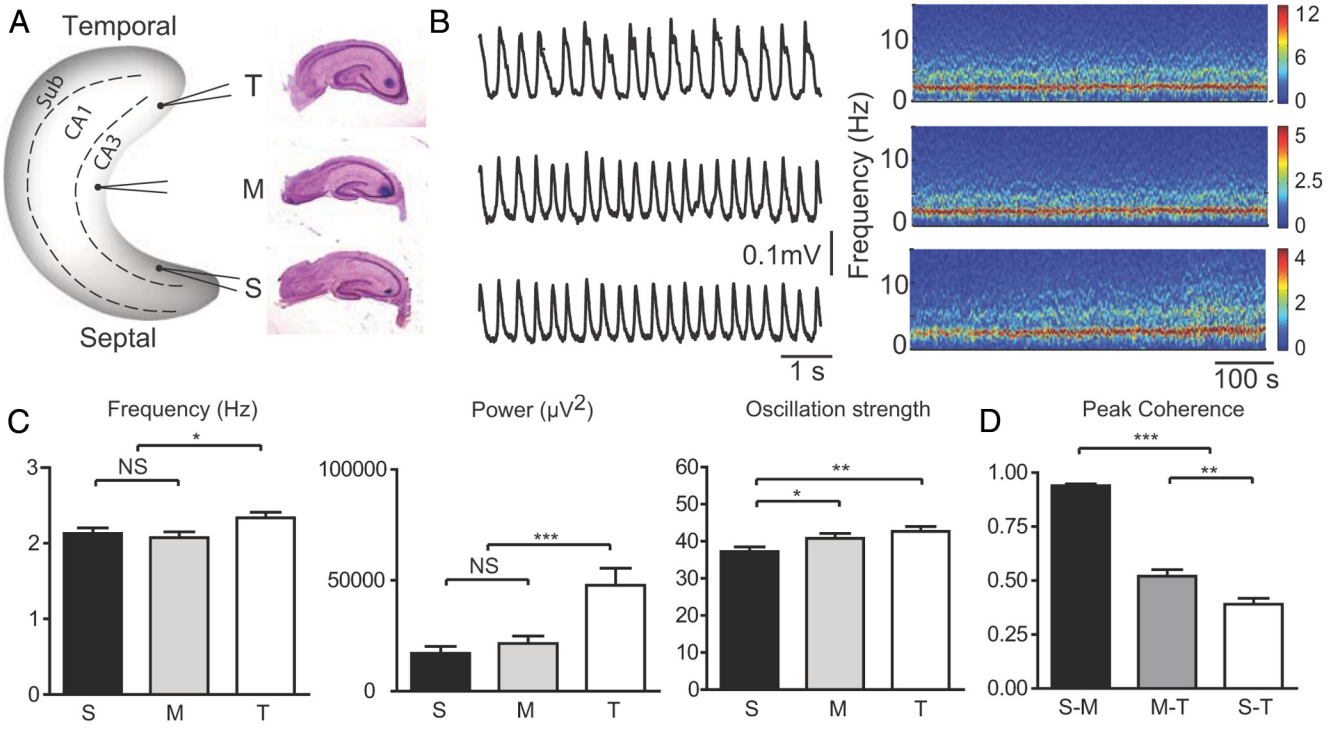

Figure 1. The properties of the CA3 oscillations. ***A***, Left, Three recording electrodes were placed in the CA3 area septally, temporally, and in intermediate region of the intact hippocampus. Right, Histological verification of the recording sites. ***B***, Left, Typical example of individual LFP traces for one experiment. Right, Spectrogram showing the power of the oscillations from the three sites. ***C***, Averaged frequency, power, and oscillation strength of the recorded rhythms from the three different locations (S, Septal; M, middle; T, temporal). Statistical analysis showed significant difference in frequency, power, and oscillation strength between septal and temporal oscillations ($n = 78$). *$p < 0.05$. **$p < 0.01$. ***$p < 0.001$. No significant differences of frequency and power were detected between middle and septal oscillations ($n = 78$; not significant, $p > 0.05$). ***D***, The septal-intermediate peak coherence (0.94 ± 0.01) was found to be significantly higher than the mediotemporal (0.52 ± 0.03) or septotemporal coherence (0.39 ± 0.03) ($n = 78$). $p < 0.001$.

spike times, and therefore reflects the strength of spike-phase locking. A similar correction for LFP waveform asymmetry was performed previously (Siapas et al., 2005). We avoid the use of circular statistics for spike–LFP relations, and instead use an entropy approach to determine the difference in entropy between the observed spike-phase distribution and the expected spike-phase distribution corrected for the wave-shape of the LFP. A similar entropy approach has been used to assess the phase–amplitude relationship between θ and γ oscillations using LFP data (Tort et al., 2010). We tested the significance of spike LFP phase locking MI by calculating the MI for a surrogate set of shuffled data. Spike–LFP MI values >2 SD above the mean of the surrogate set were judged to be significant. All results are expressed as mean ± SEM. For statistical analyses, we performed paired or unpaired Student's *t* test (two-tailed) or ANOVA using Prism (GraphPad Software). *p* values of <0.05 were considered to be statistically significant.

Materials. Sucrose, glucose, and all inorganic salts were obtained from Sigma. AMPA/kainate receptor antagonist DNQX, $GABA_A$ receptor antagonist bicuculline, NMDA receptor antagonist DL-AP5, and subunit NR2B blocker RO 25–6981 are purchased from Sigma. All drugs came from aliquots of stock solutions (stored at −80°C) and added to the perfusing artificial CSF at the concentrations indicated.

Histology. After completion of the experiment, the entire hippocampi or the CA3 strips isolated from CA1 and DG were fixed in 4% paraformaldehyde followed by sucrose until saturated. To visualize the recording electrode placement, "Chicago blue" dye were injected through the recording pipette during the end of the experiments. Tissue was cut (60 μm) at −21°C with a cryostat both in the coronal or horizontal orientation, mounted on gelatin-coated slides and stained with cresyl violet.

Results

Distinct properties of septal and temporal oscillations in CA3 area

There is substantial physiological and anatomical evidence that the septal and temporal areas of CA3 contain partly segregated networks (Swanson and Cowan, 1977; Amaral and Witter, 1989; Royer et al., 2010) with differential inputs and outputs. Our first aim was to determine the properties of endogenous network oscillations along the long axis of the CA3 area of the complete hippocampus *in vitro*. In contrast to the θ frequency (4–8 Hz) oscillations found intrinsically in areas CA1 and subiculum in the hippocampus *in vitro* (Goutagny et al., 2009; Jackson et al., 2011), the CA3 area displayed slower δ frequency (2–3 Hz) oscillations that were relatively large in power all along the septotemporal axis of CA3. The properties of the CA3 oscillations at recording sites at the septal, intermediate, and temporal regions were first characterized (Fig. 1*A*, left) at comparable depths in stratum radiatum (Fig. 1*A*, right; see Materials and Methods). Figure 1*B* shows representative recordings and spectrograms from each site (Fig. 1*B*, right). The average frequency (2.34 ± 0.08 Hz; $n = 78$), power (47.8 ± 7.6 $k\mu V^2$, $n = 78$), and oscillation strength (42.7 ± 1.3, $n = 78$) of the oscillations recorded temporally were significantly different from those recorded from the septal region (frequency, 2.13 ± 0.07 Hz, $t_{(154)} = 1.928$, $p < 0.05$; power, 17.1 ± 3.1 $k\mu V^2$, $t_{(154)} = 3.708$, $p < 0.001$; strength, 37.2 ± 1.2, $t_{(154)} = 3.055$, $p < 0.01$) (Fig. 1*C*). The average frequency and power of the oscillations at the intermediate recording site were similar to those recorded at the septal pole ($n = 78$ in each group, two sample *t* test: $p > 0.05$). The strength of the oscillations, a measure of rhythmicity, increased along the septotemporal direction (Fig. 1*C*). These results suggest that the oscillations recorded temporally have characteristics different from those recorded from the middle and septal locations. The spectral coherence of the oscillations between these recording sites revealed that the averaged peak coherence between septal and middle (S-M) oscillation was significantly higher than that from the middle and

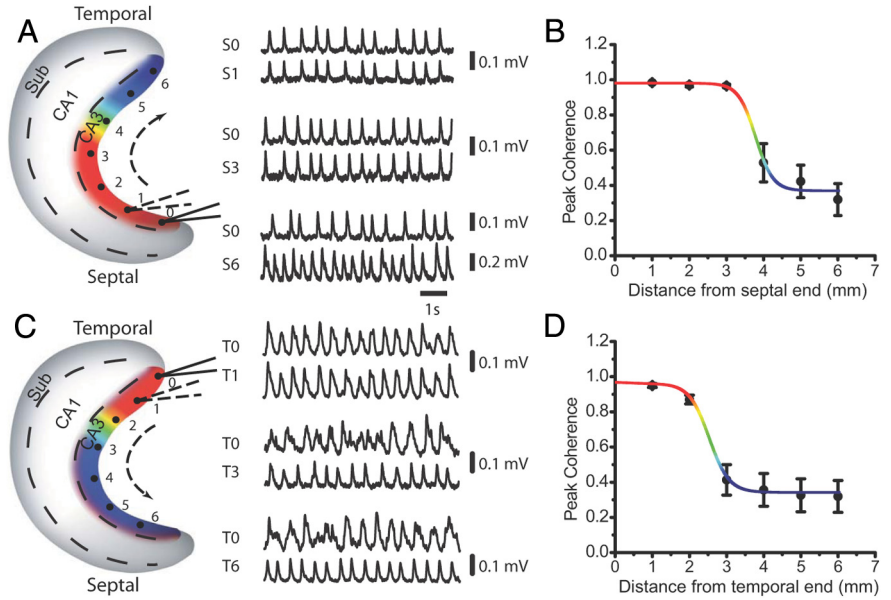

Figure 2. CA3 oscillations along the septotemporal axis. ***A***, ***C***, Seven recording sites were evenly distributed along the septotemporal (S-T) axis of the CA3 area with 1 mm interval spacing. 0, the reference electrode placed at the septal region (***A***) and temporal CA3 (***C***) end of the hippocampus. The second electrode was then moved from recording positions 1–6 to record CA3 oscillations along the septotemporal axis. Sample traces of CA3 oscillations recorded from reference electrode (0) and the second electrode (1, 3, and 6) are shown. ***B***, ***D***, averaged peak coherence was calculated between oscillations recorded from reference electrode (0) and the second electrode (1–6); $n = 7$. A sigmoid curve was then fitted based on the averaged coherence numbers with color spectrum from red (high value) to blue (low value). The color map of coherence distribution was then transferred and plotted in the CA3 area of the hippocampus model (***A***,***C***, colored area).

temporal (M-T) pairs ($t_{(154)} = 13.38$, $p < 0.0001$), whereas the septal and temporal (S-T) pairs displayed the lowest coherence (S-M, 0.94 ± 0.01; M-T, 0.52 ± 0.03; S-T, 0.39 ± 0.03) (Fig. 1*D*). These results suggest that the oscillations recorded at the septal and temporal locations arise from largely segregated networks with different properties.

The spread of network coherence in the septal and temporal networks was then determined by quantifying the changes in coherence along the longitudinal axis of CA3 (Fig. 2). The coherence was measured by comparing the oscillations recorded at one of the reference electrodes placed either at the septal (Fig. 2*A*,*B*; S0) or temporal pole (Fig. 2*C*,*D*; T0) to the oscillations recorded by another pipette displaced in 1 mm steps up to 6 mm in distance away from the reference electrode. With the reference at the septal end, the averaged peak coherence remained high (>0.9) up to a distance of 3 mm but sharply decreased near the intermediate hippocampus (Fig. 2*B*). A similar coherence measuring method was used in previous studies in the CA1 region (Bullock et al., 1990; Sabolek et al., 2009). Conversely, with the reference at the temporal end, the coherence remained high (>0.9) within 2 mm but significantly decreased 3–6 mm farther away (Fig. 2*D*). The points from averaged peak coherence were fit nicely by Boltzman sigmoidal curves ($R^2 = 0.98$, Fig. 2*B*; and $R^2 = 0.99$, Fig. 2*D*). Together, these results show that the hippocampal CA3 area contains two main oscillatory networks: a septal region measuring ~4 mm and a temporal region of 2 mm that are separated by a transition zone ($p > 0.05$, within the group; $p < 0.001$, between two groups; $n = 7$).

To determine whether the septal and temporal CA3 regions were truly autonomous oscillators, knife cuts were performed between the septal and temporal hippocampal regions. Physically separating the septal and temporal ends with a knife cut (Fig. 3*A*) abolished the septotemporal coherence from 0.39 ± 0.03 ($n = 70$) to 0.06 ± 0.004 ($n = 17$), which was below the level of statistically significant coherence ($t_{(93)} = 5.657$, $p < 0.001$; Fig. 3*B*), suggesting that the septal and temporal oscillators are weakly coupled in baseline conditions and that each region could generate oscillatory network activity autonomously without input from the other region. When the CA3 area was physically isolated (Fig. 3*C*; determined histologically; see Materials and Methods) from the dentate gyrus and CA1, no difference in septotemporal coherence was found (Fig. 3*D*) compared with uncut controls (cut, 0.30 ± 0.05, $n = 13$; uncut, 0.39 ± 0.03, $n = 70$; $p > 0.05$). In addition, the averaged frequency and power were not different in the isolated CA3 versus uncut control ($p > 0.05$). These results suggest that the level of synchrony between septal and temporal oscillators arises from activity contained within CA3.

Differential involvement of NMDA receptors in the septal and temporal oscillations

We have recently shown that intrinsically generated θ frequency rhythms in the CA1 and subiculum areas are mediated by the interplay of glutamatergic and inhibitory neurotransmission in the complete hippocampus *in vitro* (Goutagny et al., 2009; Jackson et al., 2011). Next, we determined whether glutamatergic and GABAergic mechanisms were involved in generating spontaneous CA3 oscillations. Bath application of the $GABA_A$ receptor antagonist bicuculline (2 μM) reversibly abolished both the septal and temporal CA3 oscillations within 5 min (power reduction by 96.3 ± 0.4% septally and 98.2 ± 0.3% temporally; $n = 4$ each group, paired t test, $p < 0.001$). The AMPA/kainate receptor antagonist DNQX (5 μM) also reversibly abolished CA3 oscillations at both septal and temporal CA3 regions (power reduction by: 89.4 ± 2.4% septally and 86.3 ± 4.1% temporally, compared with baseline power; $n = 4$ each group, paired t test, $p < 0.001$). These results suggest that all intrinsically generated oscillations in the complete hippocampus *in vitro* are generated by glutamate and GABA neurotransmission.

NMDA receptors are known to be essential in the induction of synaptic plasticity in hippocampus (Nakazawa et al., 2002; Rebola et al., 2010; Hunt and Castillo, 2012). Our aim was to determine whether NMDA receptors had a role in δ frequency generation and whether the role was different in septal and temporal CA3 areas of the hippocampus *in vitro*. The effects of the NMDA receptor antagonist AP-5 (50 μM) were determined on the oscillations recorded at the septal and temporal location (Fig. 4). Before AP-5 application, a close examination of the shape of the waveforms revealed a characteristic "shoulder" (Fig. 4*B*, arrow) that was more prominent temporally as indicated quantitatively by a longer decay time of the waveform ($t_{(32)} = 6.82$, $p < 0.001$; Fig. 4*C*). AP-5 application significantly increased the frequency of CA3 oscillations in the septal region (from 1.96 ± 0.09 Hz to 2.32 ± 0.16 Hz, $t_{(16)} = 3.03$, $p < 0.01$) and temporally (from 1.91 ± 0.08 Hz to 2.84 ± 0.14 Hz, Fig. 4*A*, $t_{(16)} = 11.1$, $p < 0.001$). AP-5 application also significantly reduced the "shoul-

der" and decay time of the waveform by 38.0 ± 3.7% septally (from 96.5 ± 4.7 ms to 58.0 ± 3.1 ms) and by 60.3 ± 2.7% temporally (from 154.8 ± 7.1 ms to 60.5 ± 4.7 ms; Fig. 4*B*,*C*). Both the increase in frequency and the reduction in decay time after AP-5 application were significantly more pronounced for the temporal than the septal region ($t_{(16)} = 3.39$, $p < 0.01$ for frequency increase; $t_{(16)} = 5.33$, $p < 0.001$ for decay time reduction, Figure 4*B*,*C*). To compare the contribution of NMDA receptor to the oscillations at both ends, we use the difference between the AP-5 trace and the control trace as a measure of the waveform sensitivity toward NMDA blockade. The temporal waveform consists of a larger AP-5-sensitive component than the septal waveform. As shown in Figure 4*D*, the peak amplitude and decay time of the AP-5-sensitive component are significantly higher temporally than septally, based on an analysis of a subset of the experiments (paired *t* test, peak amplitude: $t_{(4)} = 4.50$, $p < 0.05$; decay time: $t_{(4)} = 5.75$, $p < 0.01$).

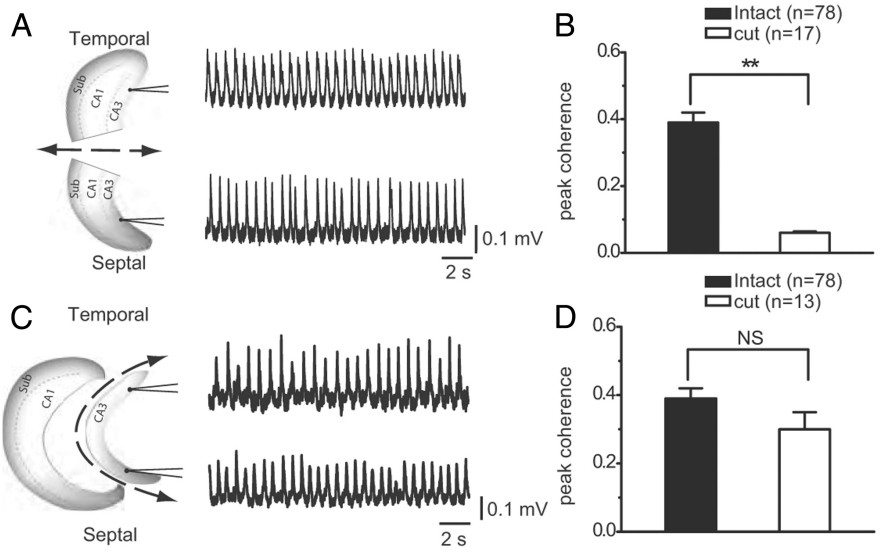

Figure 3. CA3 oscillations after the transverse or longitudinal cut. ***A***, Left, The hippocampus was cut transversely, and both ends were recorded. The sample traces from the two recording electrodes temporally and septally showing the highly rhythmic activities can be found at both ends. ***B***, Statistical analysis showing the averaged coherence ($n = 17$) between the two recording sites (septally and temporally) after the transverse cut is significantly reduced compared with the intact group ($n = 78$). $^{**}p < 0.01$. ***C***, The hippocampus was cut along the longitudinal axis to remove CA1 and DG. Sample traces were recorded from the two electrodes placed at both septal and temporal poles of the hippocampus. ***D***, The averaged coherence between the septal and temporal oscillations from the longitudinal cut group ($n = 13$) was not significantly different compared with the intact group ($n = 78$; not significant, $p > 0.05$).

We next determined whether different NMDA receptor subunits were differentially involved in CA3 rhythm generation. The NMDA receptor is a heteromeric complex composed of the NR1, and at least one of the NR2 subunits (A-D) has been shown to have distinct roles in synaptic transmission in hippocampus, whereas extrasynaptic NMDARs are predominantly NR2B type (Stocca and Vicini, 1998; Tovar and Westbrook, 1999; Scimemi et al., 2004). Activation of NR2B-containing NMDARs by synchronized synaptic input is suggested to be a means for local communication among neighboring spines (Scimemi et al., 2004). To test whether NR2B subunits contribute differentially to the temporal and septal CA3 oscillations, we bath applied the specific NR2B antagonist RO 25–6981 (Fischer et al., 1997). Similar to AP-5, RO 25–6981 significantly increased the frequency (from 1.88 ± 0.18 to 2.90 ± 0.17 Hz) and decreased the power (from 23.4 ± 6.0 to 7.8 ± 5.5 kμV^2) at the temporal, but not at the septal, recording location (Table 1). The NR2B antagonist also produced a larger decrease in the decay time of the temporal wave (from 145.2 ± 20.0 to 49.7 ± 4.3 ms) than that from the septal side (from 84.0 ± 6.7 to 65.7 ± 5.7 ms) (paired *t* test, $t_{(5)} = 4.85$, $p = 0.0012$, for the difference between septal and temporal oscillators). These results collectively show that NMDA receptors play a greater role in network rhythm generation in the temporal versus septal oscillator and the NR2B receptor is the main receptor subunit involved in mediating this effect.

Septotemporal CA3 synchronization is dependent on NMDA receptor activation

Long-lasting increases in interarea brain synchrony are thought to be important for memory-related processes because it has been proposed to promote long-term sustained communication and synaptic plasticity (Fell and Axmacher, 2011). However, it has not been directly demonstrated that NMDA receptors are involved in long-term increases in synchrony. We have taken advantage of the relatively low coherence between the CA3 septal and temporal areas to investigate whether long-term increases in coherence between septal and temporal areas can be induced through NMDA receptor-dependent mechanisms. Previous work has shown that the temporal (or ventral) NMDA receptors in the hippocampus are important for the expression of anxiogenic states during elevated plus maze (Nascimento Häckl and Carobrez, 2007). Based on the finding that an important NMDA component is present during the δ oscillations (especially on the temporal CA3 region), we next determined whether CA3 septal-temporal coherence could be increased in an NMDA receptor-dependent manner. To test this, extracellular Ca^{2+} concentration was raised from 2 to 4 mM for a short 3 min duration. This is a classic paradigm previously shown to induce LTP in hippocampal slices (Turner et al., 1982; Reymann et al., 1986; Melchers et al., 1987). Interestingly, transiently increasing Ca^{2+} concentrations significantly and irreversibly potentiated the peak coherence between septal and temporal CA3 oscillations from 0.35 ± 0.08 during baseline to 0.77 ± 0.05 (paired *t* test, $t_{(5)} = 4.85$, $p < 0.01$) for >40 min after calcium returned to baseline levels (Fig. 5). It was next determined whether the increase in synchrony was dependent on NMDA receptor activation. When AP-5 (50 μM) was applied concomitantly with the increase in extracellular calcium, the long-lasting potentiation in coherence was prevented, showing that the calcium-induced coherence potentiation was the result of NMDA receptor activation (Fig. 5*A*,*B*). The transient Ca^{2+} increase augmented the power of septal and temporal oscillations (Fig. 5*C*, solid points) but failed to have significant effects on the frequency or rhythmicity of the oscillations (data not shown). An increase in power was also measured when calcium was coapplied with AP-5 (Fig. 5*C*), suggesting that an NMDA-receptor independent mechanism underlies the change in LFP power. To analyze whether the change in coherence was the result of increases in power or phase locking between the oscillators, we analyzed the PLV (Le Van Quyen and Bragin,

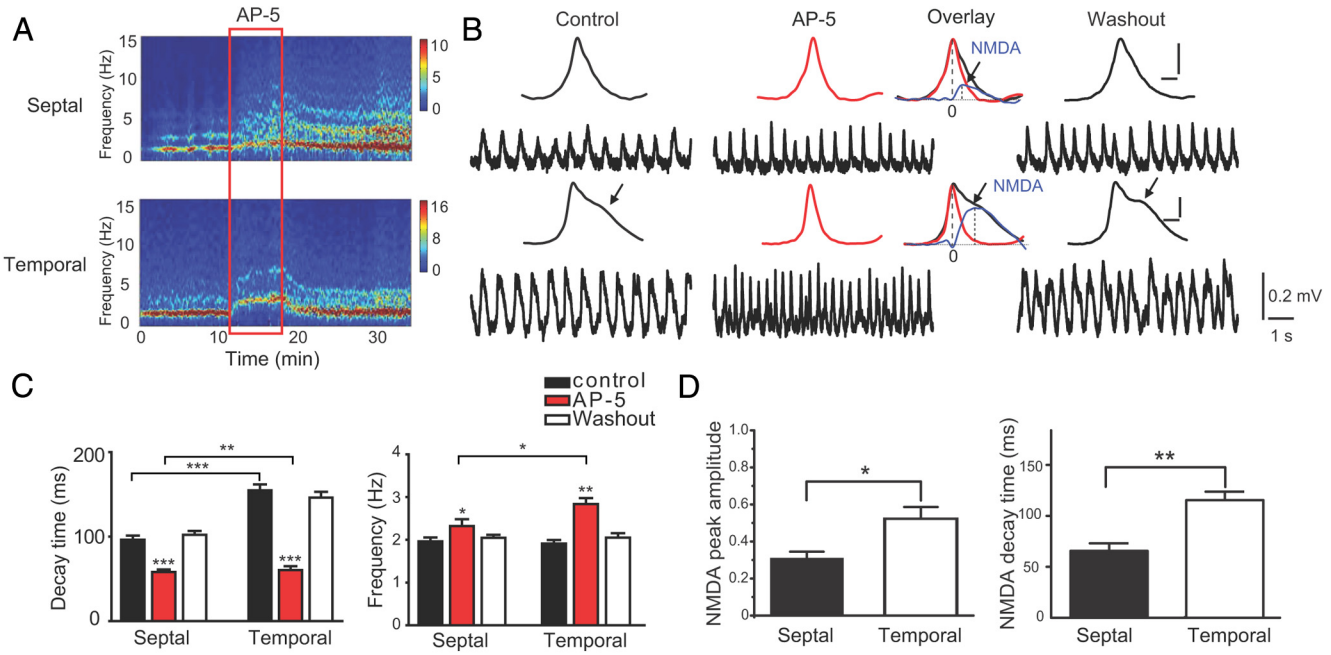

Figure 4. Differential effect of AP-5 on CA3 oscillations. ***A***, Sample spectrogram showing that NMDA receptor blockade by AP-5 significantly increased the frequency of CA3 oscillation temporally, in clear contrast to the mild increase of the frequency in septal site. ***B***, Representative traces from the same recording in ***A***, showing CA3 oscillations at septal and temporal poles in control (left), application of NMDA receptor antagonist AP-5 (middle) and washout (right) condition. Insets, Averaged waveforms taken from 1-min-long sample traces. The temporal oscillations often have "shoulders" (see arrows) in control and washout condition. Application of AP-5 eliminated the shoulder and narrowed the waveform (middle inset). An AP-5-sensitive component (blue trace) was the result of the differences between the AP-5 trace and the control trace (inset scale: *x*, 100 ms; *y*, 0.1 mV). ***C***, Left, Statistics showed that AP-5 significantly decreased the decay time of the averaged waveform from both septal and temporal oscillations with a differential decrease rate. Right, Bar graphs show that AP-5 increased the dorsal and ventral oscillation frequency with a greater effect on the temporal oscillator. ***D***, Statistics showed a significant difference in the AP-5-sensitive component septally versus temporally. Left, The normalized peak amplitude (temporal, 0.52 ± 0.06; septal, 0.30 ± 0.04). Right, The decay time of the AP-5-sensitive component (temporal, 114.8 ± 8.3 ms; septal, 65.5 ± 7.4 ms). For all analyses: *$p < 0.05$, **$p < 0.01$, ***$p < 0.001$).

Table 1. Comparison of AP-5 and RO effect on CA3 oscillations

	AP-5 (50 μM)		RO 25-6981 (5 μM)	
	Septal	Temporal	Septal	Temporal
Waveform amplitude (mV)	0.11 ± 0.02 to 0.10 ± 0.02	0.22 ± 0.02 to 0.23 ± 0.03	0.12 ± 0.03 to 0.11 ± 0.03	0.31 ± 0.07 to 0.21 ± 0.07
	NS	NS	NS	NS
Waveform rising time (ms)	114.7 ± 6.6 to 124.5 ± 11.8	136.1 ± 9.5 to 119.9 ± 8.4	136.7 ± 14.7 to 126.0 ± 15.1	116.7 ± 11.6 to 98.3 ± 8.5
	NS	NS	NS	NS
Waveform decay time (ms)	96.5 ± 4.7 to 58.0 ± 3.1	154.8 ± 7.1 to 60.5 ± 4.7	84.0 ± 6.7 to 65.7 ± 5.7	145.2 ± 20.0 to 49.7 ± 4.3
	***	***	**	**
Oscillation frequency (Hz)	↓ ↓ ↓ (38.0 ± 3.7%) 1.96 ± 0.09 to 2.32 ± 0.16	↓ ↓ ↓ (60.3 ± 2.7%) 1.91 ± 0.08 to 2.84 ± 0.14	↓ (20.4 ± 6.7%) 2.22 ± 0.14 to 2.42 ± 0.27	↓ ↓ (61.4 ± 6.2%) 1.88 ± 0.18 to 2.90 ± 0.17
	***	***	*	*
Oscillation power (kμV^2)	↑ ↑ (17.9 ± 7.3%) 11.5 ± 2.1 to 6.4 ± 1.2	↑ ↑ ↑ (48.7 ± 4.1%) 52.3 ± 8.8 to 41.6 ± 8.1	NS	↑ (61.1 ± 21.8%)
	NS	NS	*	*
Oscillation strength	↓ ↓ (38.8 ± 8.7%) 37.3 ± 2.8 to 27.2 ± 1.9	↓ (22.7 ± 9.6%) 52.7 ± 2.3 to 37.3 ± 2.0	NS 40.1 ± 7.2 to 33.5 ± 7.0	↓ ↓ (66.5 ± 17.1%) 38.9 ± 3.6 to 27.8 ± 5.3
	NS	NS	*	*
	↓ ↓ ↓ (23.2 ± 6.5%)	↓ ↓ ↓ (28.3 ± 3.6%)	NS	↓ (28.9 ± 10.9%)

↑ indicates Significant increase; ↓ , significant decrease. 1 arrow, $p < 0.05$; 2 arrows, $p < 0.01$; 3 arrows, $p < 0.001$. NS, not significant ($p > 0.05$, paired *t* test). AP-5, $n = 17$; RO, $n = 6$.
Significant differential effect septal versus temporal test: *$p < 0.05$; **$p < 0.01$; ***$p < 0.001$; NS, $p > 0.05$.

2007) between septal and temporal oscillations. A comparable enhancement of the PLV by extracellular calcium elevation was also observed, suggesting that the increase in spectral coherence was mediated by increased phase–phase synchrony and not power alone (Fig. 5*D*, solid points). The long-lasting potentiation in the PLV was prevented by the application of AP-5 during high Ca^{2+}, similar to coherence (Fig. 5*D*).

Together, these results show that short bath application of extracellular calcium produces long-lasting increases in both phase synchrony as well as LFP power. Which factor is more responsible for the long-lasting coherence increase? To address this question, we extracted the (late) coherence value 24–25 min after the calcium induction and correlated the data with the (early) PLVs and power values during the 3 min high Ca^{2+} application from all the experiments (Ca^{2+} alone and Ca^{2+} coapplied with AP-5). We found a strong correlation between the early PLV and late peak coherence ($n = 16$, linear fit: $r = 0.76$, $p < 0.001$). However, no correlation was found between early power increase and later coherence increase

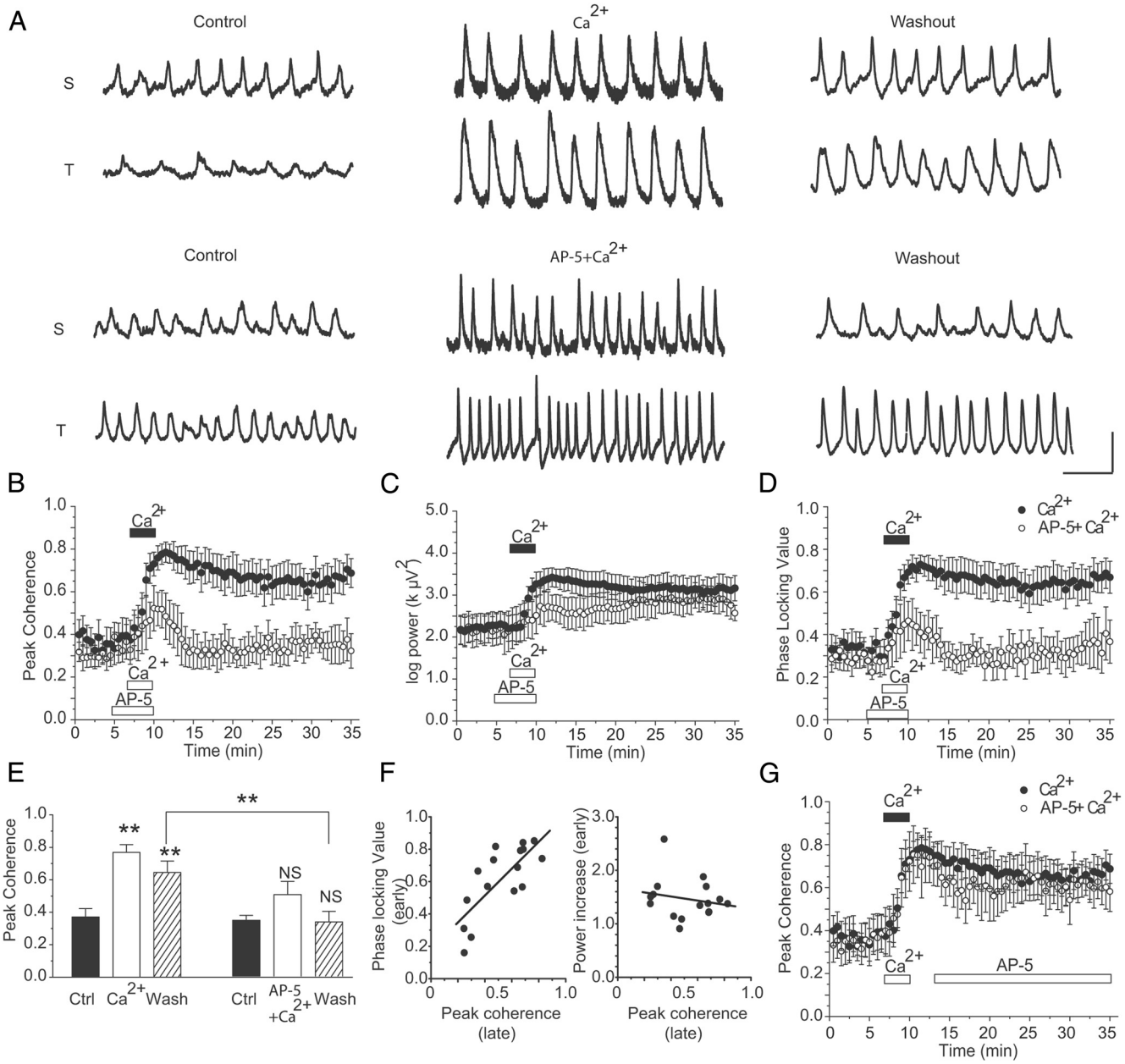

Figure 5. NMDA-dependent septotemporal coherence plasticity. ***A***, Representative traces. Top, In control conditions, the septal and temporal oscillations exhibit low coherence, whereas during high $[Ca]_o$ and the washout period, the two oscillations become highly coherent. Bottom, Representative traces from the septal and temporal oscillators in control, high $[Ca]_o$ with AP-5, and washout period. There is a visible lack of coupling during and after $[Ca^{2+}]o$. ***B***, Time course of peak coherence. Solid points indicate averaged peak coherence showing the "LTP"-like effect induced by high calcium; hollow points, averaged coherence shown while NMDA channels are blocked by preapplication of AP-5 (50 μM), subsequent high calcium application failed to induce the S-T coherence potentiation. ***C***, ***D***, The time course of power and PLV during the high calcium (solid points) experiments or during high calcium with AP-5 (hollow points). ***E***, Summary graph of peak coherence change by high calcium (left) or by high calcium with AP-5 (right); each group, $n = 6$. $^{**}p < 0.01$. NS, Not significant ($p > 0.05$). ***F***, Linear regression graph. Left, Coherence value 24–25 min after washout versus PLV during 3 min high calcium induction. Right, Coherence value 24–25 min after washout versus power value during 3 min high calcium induction. ***G***, Averaged coherence showing that, after the high calcium potentiation of S-T coherence, subsequent application of NMDA channel blocker AP-5 had no significant effect on the potentiated coherence (hollowed points) compared with that without AP-5 presence (solid points).

($n = 16$, linear fit: $r = -0.19$, $p > 0.05$; Fig. 5*F*). Therefore, we propose that the increased phase–phase synchronization during high calcium is responsible for the long-lasting changes in coherence between septal and temporal oscillators. The significant potentiation in coherence was not changed when AP-5 was applied after the calcium increase (0.29 ± 0.05 to 0.54 ± 0.11; paired t test, $n = 5$, $p < 0.01$; Fig. 5*G*, hollow points). These results suggest that, once NMDA receptors are activated, the increase in coherence becomes independent of NMDA receptors, a phenomenon reminiscent to the NMDA-dependent LTP mechanism in hippocampus. As an additional control, a similar increase in coherence was observed by perfusing an artificial CSF containing low magnesium ($MgSO_4$: 1 mM from 2 mM) instead of high calcium to activate the NMDA receptors (baseline coherence: 0.21 ± 0.04; after low Mg^{2+} at 25 min: 0.52 ± 0.1; $n = 4$, paired t test, $p < 0.05$).

High $[Ca^{2+}]_O$ effect on the local and distal unit firing properties

In addition to LFP phase–phase synchronization between septal and temporal CA3 regions, we aimed to determine whether there was an

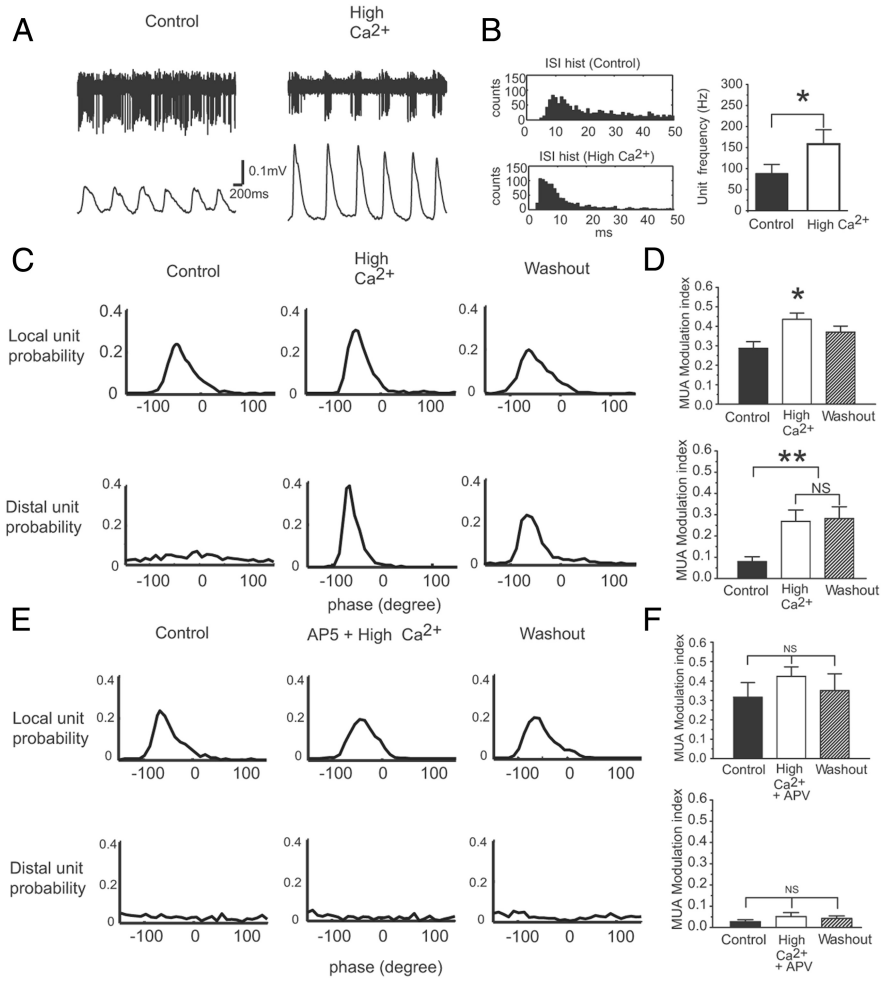

Figure 6. High $[Ca^{2+}]_o$ synchronized distal unit firing in relation to the local field potential oscillation. ***A***, Sample recording of unit firing in relation to the local field oscillation in control and high $[Ca^{2+}]_o$ condition. ***B***, Statistical data showing high $[Ca^{2+}]_o$ increased the bursting frequency. Left, The interspike interval histogram. Right, The mean burst frequency from the group data. *$p < 0.05$. ***C***, Top, Sample histogram showing probability distribution of the local units within each phase bin of the averaged LFP waveform from 2 min during control, high $[Ca^{2+}]_o$, and washout periods. The peak of each waveform recorded from stratum radiatum is 0 degrees. Bottom, Histogram showing the probability distribution of the distally recorded units referenced to the same LFP phase as above. The lack of phase modulation of the distal unit activity during baseline conditions and subsequent increase in phase modulation during high calcium and washout conditions. ***D***, Group data for spike-field MI. Top, High $[Ca^{2+}]_o$ effect on unit (local)–field (local) phase locking. Bottom, High $[Ca^{2+}]_o$ effect on unit (distal)–field (local) phase locking with little/no effect of washout. *$p < 0.05$; **$p < 0.01$. NS, Not significant. ***E***, Similar to ***C***, only during experiments where high $[Ca^{2+}]_o$ was bath applied with 50 μM AP-5 3 min before the high $[Ca^{2+}]_o$. Under this condition, the spike-phase MI displayed no clear difference between control versus high calcium and washout condition. ***F***, Summary graph showing that preapplication of 50 μM AP-5, before high $[Ca^{2+}]_o$ blocked the increase in spike-phase MI both locally and distally.

increase of the phase locking between local spikes and the distal LFPs at both CA3 septal and temporal region. When local spikes were recorded at the septal region of the CA3, the distal LFPs were collected at the temporal part, and vice versa. Not surprisingly, during baseline conditions, spikes in one region were widely distributed across the phase of the LFP recorded in the other region (septal or temporal) demonstrating low measures of spike–LFP phase locking. In the period after high $[Ca^{2+}]_O$ application, the spike–LFP phase locking was increased (from 0.08 ± 0.03 to 0.25 ± 0.04, paired *t* test, $n = 4$, $p < 0.01$). After high $[Ca^{2+}]_O$ condition, we found that the total number of spikes was not significantly changed; however, the first-order interspike interval of CA3 pyramidal cell bursting was decreased (corresponding to 88.0 ± 22 Hz to 158.2 ± 34 Hz, paired *t* test, $n = 4$, $p < 0.01$) during each cycle (Fig. 6*A*,*B*).

The effects of high $[Ca^{2+}]_o$ on multiunit activities (MUAs) recorded locally and distally were also investigated. The phase locking of both local and distal MUA to the local LFP was determined. For this analysis, we pooled all data from septal and temporal recordings, where local spiking was considered those neurons recorded within 0.1 mm of the LFP reference, and distal MUA was recorded at the opposite hippocampal region. The spike phase locking was determined by first generating the spike-phase probability distribution. Again, after correcting for asymmetry in the LFP wave shape, the depth of spike–LFP phase MI was calculated (see Materials and Methods). We found, in control conditions, that the local MUAs are highly modulated by the phase of the local field oscillation, whereas the distal MUAs had relatively low phase locking to the same reference field signal (Fig. 6*C*,*E*, left column). During 3 min application of $[Ca^{2+}]_O$, distal MUAs are significantly synchronized and become highly modulated by the reference field (MI = 0.08 ± 0.02 to 0.27 ± 0.05, paired *t* test, $n = 5$, $p < 0.01$; Fig. 6*C*, middle), and the spike field MI remained high at 0.28 ± 0.05 during washout (Fig. 6*C*,*D*, bottom). We also found an increase in the MI (from 0.30 ± 0.03 to 0.43 ± 0.03, paired *t* test, $n = 5$, $p < 0.05$) between local spikes and local LFPs by $[Ca^{2+}]_o$, and this effect was reversed by washout (0.36 ± 0.03) (Fig. 6*C*,*D*, top). When AP-5 was coapplied with $[Ca^{2+}]_o$ distal spikes failed to synchronize with the local field (Fig. 6*E*,*F*), as the MI did not change relative to baseline conditions (control: 0.023 ± 0.009; AP-5 with high $[Ca^{2+}]_o$: 0.047 ± 0.017; washout: 0.038 ± 0.011; $n = 5$ in each group, one-way ANOVA, $p > 0.05$) (Fig. 6*E*, bottom).

Reversal of septotemporal direction during phase synchronization via activation of NMDArs

The septal and temporal oscillators represent a system of weakly coupled oscillators. These oscillators are therefore interacting or communicating through phase synchronization. We wanted to determine whether there was a consistent direction with which the coupling was arising, by calculating the PLV after analytically introducing a time lag ($\tau = -1{:}{+}1$ s, in 5 ms steps) to the septal oscillator (Fig. 7*A*). Therefore, the PLV is calculated at 401 points at each specified time lag and the lag where the maximal synchronization occurs is reported (PLV-shift). The PLV-shift technique assesses the magnitude of phase–phase synchrony between two time series vectors as a function of time lags between two signals and is similar to the Z-shift technique reported previously (Siapas et al., 2005; Hangya et al., 2009), except that the PLV is a normalized measure between 0 and 1. During the baseline condition, the PLV-shift was found at 36.1 ± 15 ms (septal leading the temporal oscillator). During high $[Ca^{2+}]_o$ when phase–phase synchrony is increased, the PLV-shift was found to be changed to −8.3 ± 14.8

ms ($n = 6$, paired t test, $p < 0.05$). This low value (close to 0 ms) of the PLV-shift suggests that there is strong bidirectional communication between oscillators during high calcium. Interestingly, after the washout when the system exhibited the sustained plastic changes in coherence, the PLV-shift was changed to -24.8 ± 26.2 ms demonstrating maximal synchronization in the temporal to septal direction. Therefore, the plasticity-associated increase in coherence was driven by a change in the dynamics of intra-CA3 connectivity and a shift in the direction of phase coupling from "septal-temporal" (S $\rightarrow$ T) in control condition to "temporal to septal" (T $\rightarrow$ S) after NMDA receptor activation (Fig. 7*B*). When the NMDA-dependent coupling process was blocked by coapplying AP-5 (50 μM) during the high $[Ca^{2+}]_O$, no plastic change of PLV-shift was found (control, 49 $\pm$ 63.7 ms; washout, 82 $\pm$ 119.6 ms, $n = 5$, paired t test: $p > 0.05$; Fig. 7*C*). In addition, once the phase locking process was initiated by high $[Ca^{2+}]_O$, later application of AP-5 did not reduce the PLV-shift back to control conditions (control, 103.3 $\pm$ 75.4 ms; washout, -162.9 ± 44.7 ms, $n = 4$, paired t test: $p < 0.05$; Fig. 7*D*). To summarize the above findings, weak coupling during baseline conditions in aCSF is associated with a (S $\rightarrow$ T) direction of phase synchrony, and NMDAr activation increases in phase coupling and exerts a long-lasting plasticity-associated switch in the direction of information flow favoring a (T $\rightarrow$ S) direction (Fig. 7*E*).

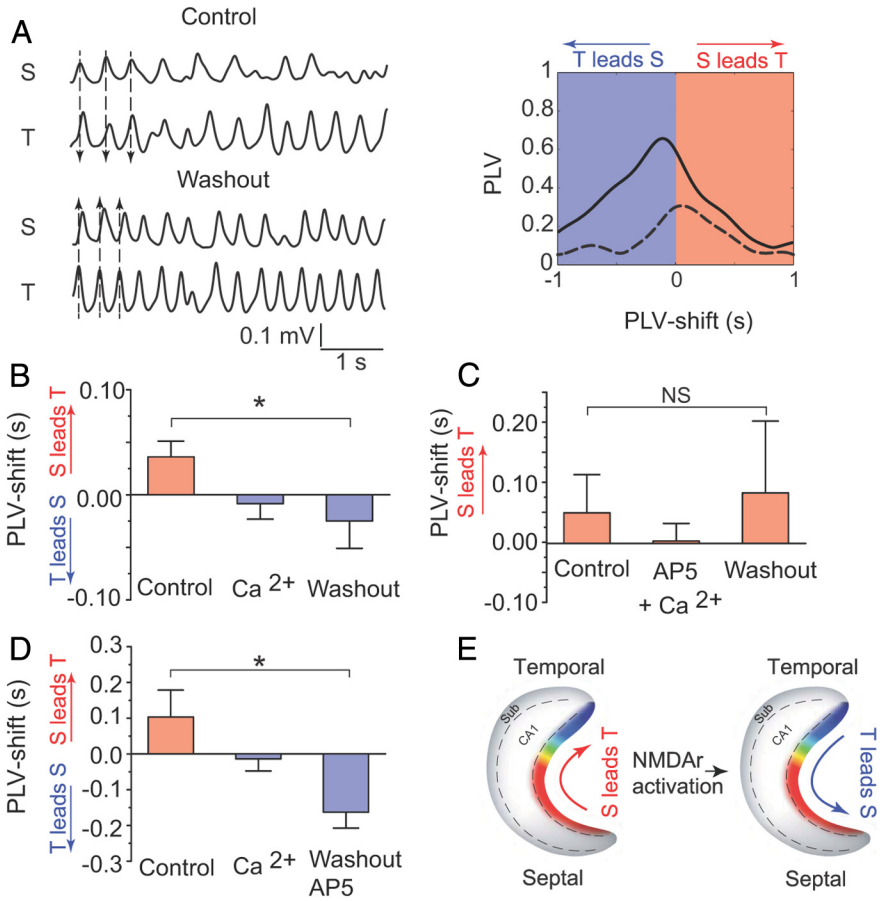

Figure 7. Dynamic changes in phase locking between septal and temporal oscillators. ***A***, Left, Representative traces filtered in the 0.5–10 Hz band showing in control condition that the septal oscillation leads slightly ahead of the temporal oscillation; 20 min after washout of the high calcium application, the temporal oscillation leads the septal oscillator (dashed arrow lines). Right, Sample results of the PLV calculated using the mean resultant length of the phase difference (in radians) between vectors. If the maximum PLV occurred >0 s, then the temporal oscillator was most phase-locked to the past history of the septal oscillator; therefore, the septal oscillator is said to lead the temporal oscillator (dashed line; control condition). Conversely, if the PLV plot exhibits a peak in the region <0 s, then the temporal oscillator can be said to lead the septal oscillator (solid line; during washout). All analysis was performed on 2 min data segments. ***B***, In the control group, the averaged phase shift time is 36.1 $\pm$ 15 ms, indicating that the septal oscillation is leading the temporal one. The averaged values during high calcium application and washout are -8.3 ± 14.8 ms and -24.8 ± 26.2 ms, respectively, suggesting that the temporal oscillation is leading the septal region ($n = 6$). *$p < 0.05$. ***C***, When 50 μM AP-5 is applied before high calcium application, the averaged phase shift times in control, high calcium, and washout period are 49 $\pm$ 63.7, 2 $\pm$ 29.4, and 82 $\pm$ 119.6 ms, respectively, suggesting that, without NMDAr activation, the septal oscillations tend to lead the temporal ones ($n = 5$). NS, Not significant. ***D***, When AP-5 was applied during the washout of the high calcium, the averaged phase shift time is 103.3 $\pm$ 75.4 ms in the control group, whereas high calcium application reduced the phase shift time to -13.8 ± 33.9 ms, and further to -162.9 ± 44.7 ms during washout in the presence of AP-5, suggesting a change of the directionality over the phase locking process ($n = 4$). *$p < 0.05$. ***E***, Diagram summarizes the finding that increasing the PLV by activation of the NMDAr can reverse the directionality between septal and temporal oscillations.

Discussion

Our study has shown that both septal and temporal poles of the hippocampal CA3 region have independent δ frequency oscillators. These oscillators were both synaptically generated by ionotropic glutamate and fast GABAergic mechanisms but had a differential dependence on NMDA receptor activity. The dependence and modulation of these oscillators by NMDA receptor activity suggest that oscillations have a role in shaping plasticity. Systematically increasing synaptic transmission and spiking by transiently increasing extracellular calcium led to a long-term NMDA receptor-dependent enhancement of the coherence between both oscillators, and synchronized both local and distal unit firing activities. Furthermore, we found that, in baseline conditions, the septal CA3 was leading the temporal CA3, and NMDA receptor activation switched this directionality. Our results provide evidence for long range hippocampal communication and potential interactions between spatial navigation and motivational behavior related brain regions, using NMDA-dependent phase synchronization.

There is increasing evidence that the septal and temporal hippocampus is different in terms of the genes they express, their connectivity, and their function (Moser et al., 1993; Bannerman et al., 1999; Kjelstrup et al., 2002; Pentkowski et al., 2006; Fanselow and Dong, 2010). However, whether the septal and temporal poles contain intrinsically separable networks remains unclear. Indeed, previous work has shown that the septal and temporal CA3 networks might be relatively independent because they show low synchronization in the θ frequency range (Royer et al., 2010), a sign that, under basal conditions, the synaptic interactions between the two regions are weak. However, the poor synchronization between these oscillators *in vivo* may be the result of differential input from the entorhinal cortex or another region, which may differentially synchronize the septal and temporal regions, resulting in low synchrony. In the isolated hippocampus *in vitro*, the oscillations recorded temporally in CA3 displayed sustained δ frequency rhythms that were significantly

faster in frequency, larger in power, and more rhythmic than those in the septal CA3. Moreover, we found that the CA3 septotemporal δ frequency coherence in the isolated hippocampus was comparable (0.3–0.4) to the θ coherence measured septotemporally in the CA3 area *in vivo* (Royer et al., 2010). In addition, the time lag between septal and temporal synchronization (<80 ms) was similar to the delay between CA1 septal and temporal regions found *in vivo* (Patel et al., 2012), suggesting that similar CA3 time lags may be found *in vivo*. More interesting was the finding that the NMDA receptors (especially those containing the NR2B subunits) had a much larger contribution to the temporal CA3 area oscillations than those recorded septally. A similar predominance of NMDA receptor-mediated components of electrically elicited EPSPs or low-Mg^{2+}-induced bursting were also reported in hippocampal slices recorded from the CA3 temporal area (Papatheodoropoulos et al., 2005). Although it is well established that NR2B subunits are crucial for implementing Hebb's rule and gating synaptic plasticity in the hippocampus (Tang et al., 1999; Liu et al., 2004), other evidence suggests that NR2B subunit expression in hippocampus and amygdala is found to be closely related to animal anxiety (Lehner et al., 2011). It has been shown that temporal, but not septal, hippocampal NMDA receptors have an important role in regulating anxiety because infusion of NMDA receptor antagonists into the temporal hippocampus produces an impairment in the expression of anxiety and defensive behaviors (Nascimento Häckl and Carobrez, 2007; Barkus et al., 2010). Therefore, it is possible that activation of NMDA receptors in the ventral hippocampus during anxiety plays an important role in shaping local circuit activity to communicate with the dorsal hippocampus, and other extrahippocampal structures. Phase–phase coupling with the dorsal hippocampus would assist in merging different aspects of environmental context into a unified memory trace. Our *in vitro* results clearly demonstrate that the low synchronization between the two CA3 areas is not a result of differential input to the septal and temporal areas (e.g., from entorhinal cortex) as the hippocampus is isolated. Together, our results further suggest that CA3 septal and temporal areas have distinct properties and are weakly communicating under baseline spontaneous conditions. This segregation of septal and temporal networks could support differential processing of information relevant for spatial (septal CA3), and emotional (temporal CA3) functions (Bannerman et al., 1999, 2003; Kjelstrup et al., 2002), and the integration of these different processes may occur through NMDA-dependent phase-coupling.

Role of NMDA receptors in coherence

Increases in coherence can occur transiently to support rapid information exchange between brain areas but can also be long-lasting to promote sustained communication that may support synaptic plasticity required for memory processes (Fell and Axmacher, 2011). Whereas high-frequency oscillation reflects local processing, low-frequency brain rhythms are dynamically entrained across distributed brain regions. In the human brain, the phase synchronization of neuronal activities between regions is crucial for working memory (Palva et al., 2005; Fujisawa and Buzsáki, 2011) as well as episodic memory encoding and retrieval (Rodriguez et al., 1999; Canolty et al., 2006; Watrous et al., 2013). In humans, the hippocampus serves as a hub mediating memory retrieval by phase synchronization with different cortical targets (Watrous et al., 2013). Therefore, perhaps this rapid and efficient δ–θ synchrony between regions during retrieval is facilitated by strengthened connections established by NMDA-dependent phase coupling. Long-term increases in coherence at θ frequency have been shown to occur between the hippocampus and prefrontal cortex and is associated with successful working memory encoding and maintenance (Siapas et al., 2005; Benchenane et al., 2010; Sigurdsson et al., 2010; Fujisawa and Buzsáki, 2011). Such long-lasting increases in coherence have also been observed between the hippocampus and the amygdala (fear conditioning; Popa et al., 2010), striatum (procedural learning; DeCoteau et al., 2007) and between other regions, such as entorhinal cortex and prefrontal cortex (Takehara-Nishiuchi et al., 2011). The increase in coherence between brain regions is thought to underlie interregional spike alignment and coordination for optimizing neuronal communication (Fries, 2005; Womelsdorf et al., 2007). This coordination of spiking will likely promote Hebbian learning, such that presynaptic neurons will favorably increase postsynaptic depolarization and induce synaptic plasticity if the postsynaptic neuron is receiving inputs at the optimal phase. However, there is little evidence at the cellular level that increases in phase locking can trigger NMDA receptor-dependent long-term potentiation in coherence. Our data suggest that NMDA receptor activation through synaptic plasticity can promote long-term increases in septotemporal coherence. Transient increases in calcium triggered a dramatic NMDA receptor-dependent long-lasting increase in the CA3 septotemporal coherence that was predominantly the result of an increase in the phase locking between the oscillators. Therefore, we think that phase locking itself is the necessary requirement for inducing the long-term changes in coherence and communication between septal and temporal regions. This synchrony may be supported partly by axonal projections along the CA3 longitudinal axis made by CA3 pyramidal cells (Li et al., 1994).

When the spiking dynamics were investigated, it was found that the calcium-induced increase in phase synchronization was associated with an increase in the phase locking of CA3 pyramidal cells across the dorsal ventral axis (Fig. 6). NMDA receptor blockade did not alter the increase in spike-field coherence locally but blocked the interarea increase in spike-field coherence, suggesting that NMDA receptors are necessary for the long-term coupling of the interarea spike-field coherence. Interestingly, a recent study also showed that an NMDA antagonist (ketamine) could disrupt the θ coherence along the septotemporal axis of the CA1 region (Hinman et al., 2013), providing *in vivo* evidence of NMDA receptor involvement in hippocampal network synchronization. In addition to inducing a long-term increase in coherence and phase locking, the activation of NMDA receptors also changed the direction of oscillator influence from a septal to temporal direction in control to a temporal septal direction after NMDA receptor activation. This shift in direction of synchronization likely arises because of the increased NMDA component in the ventral CA3 region, which would promote relatively greater population synchrony and consequently increase the strength of the outputs to the septal CA3. However, a combination of both presynaptic and postsynaptic mechanisms are likely involved.

A surprising aspect of the present study is the spectral properties of the intrinsic septotemporal oscillators. In our previous study, we have shown that the oscillations recorded in the CA1 area (Goutagny et al., 2009) and in the subiculum (Jackson et al., 2011) display relatively faster frequency oscillations well within the θ frequency range of 4–8 Hz. These oscillations were generated by prominent phasic IPSPs in pyramidal cells, which could trigger postinhibitory rebound spiking. In contrast, the oscillations in the CA3 were relatively slow (2–3 Hz) and were mediated by large EPSPs triggering a few spikes; whereas the inhibition, although essential in the generation of this rhythm, appeared

more subtle and masked by the excitation. Such slow oscillations with similar mechanisms were also noted previously (Wu et al., 2006) using a complete hippocampal preparation *in vitro*. Therefore, it appears that the properties of the CA3 oscillations are significantly different from those of the CA1 or subiculum. δ oscillations occur in the hippocampus during nREM sleep (Isomura et al., 2006; Wolansky et al., 2006). Therefore, this δ frequency communication between septal and temporal CA3 regions may occur mostly during sleep-dependent memory consolidation (Marshall and Born, 2007). Alternatively, CA3 δ frequencies may be important for communicating with other regions, such as the lateral entorhinal cortex (Deshmukh et al., 2010) and ventral tegmental area (Fujisawa and Buzsáki, 2011), which exhibit task-dependent δ frequencies in the freely moving animal. The frequency of LFPs recorded *in vivo* is likely a product of intrinsic cell and circuit properties, which can be modulated by the level of synaptic input from the medial septum (Fellous and Sejnowski, 2000) and entorhinal cortex. Increased level of cholinergic drive was found previously to switch δ frequency oscillations to the θ frequency (Fellous and Sejnowski, 2000). In addition, cholinergic lesions of the MS produce a δ frequency rhythm within the hippocampus (Lee et al., 1994). These results suggest that CA3 δ rhythms may arise from reduced excitatory (cholinergic) or disinhibitory (GABAergic) septal inputs. Although most work has focused on θ frequencies in CA3, δ frequencies are coexpressed with θ and may play a different or complementary role in mediating circuit computations. We suggest that an input to CA3 is necessary to shift the slow intrinsic oscillator into the θ range. In addition to the medial septum, the hippocampal CA3 area receives inputs originating from stellate cells in layer II of the medial entorhinal cortex, which have intrinsic θ resonant properties (Alonso and Llinás, 1989; Giocomo et al., 2007). These entorhinal θ inputs could also have a role in transforming the δ rhythm to the θ range providing and explanation for the strong cortical-CA3 θ coherence seen *in vivo* (Mizuseki et al., 2009).

In conclusion, we have shown that the septal and temporal CA3 regions possess dissociable oscillators that have slightly different spectral properties and dependence on NMDA receptor activation. These oscillators are weakly coupled under baseline conditions; but upon activation of NMDA receptors, these oscillators become highly coupled; and this coupling persists long after the activation is terminated, therefore resembling an LTP-like phenomenon with neural oscillations. These results suggest binding of neural activity in functionally dissociable brain regions through NMDA-dependent phase locking could serve as a mechanism for linking emotional and spatial memory related information in hippocampal networks.

References

Adhikari A, Topiwala MA, Gordon JA (2011) Single units in the medial prefrontal cortex with anxiety-related firing patterns are preferentially influenced by ventral hippocampal activity. Neuron 71:898–910. CrossRef Medline

Alonso A, Llinás RR (1989) Subthreshold Na+-dependent θ-like rhythmicity in stellate cells of entorhinal cortex layer II. Nature 342:175–177. CrossRef Medline

Amaral DG, Witter MP (1989) The three-dimensional organization of the hippocampal formation: a review of anatomical data. Neuroscience 31: 571–591. CrossRef Medline

Bannerman DM, Yee BK, Good MA, Heupel MJ, Iversen SD, Rawlins JN (1999) Double dissociation of function within the hippocampus: a comparison of dorsal, ventral, and complete hippocampal cytotoxic lesions. Behav Neurosci 113:1170–1188. CrossRef Medline

Bannerman DM, Grubb M, Deacon RM, Yee BK, Feldon J, Rawlins JN (2003) Ventral hippocampal lesions affect anxiety but not spatial learning. Behav Brain Res 139:197–213. CrossRef Medline

Barkus C, McHugh SB, Sprengel R, Seeburg PH, Rawlins JN, Bannerman DM (2010) Hippocampal NMDA receptors and anxiety: at the interface between cognition and emotion. Eur J Pharmacol 626:49–56. CrossRef Medline

Bast T, Wilson IA, Witter MP, Morris RG (2009) From rapid place learning to behavioral performance: a key role for the intermediate hippocampus. PLoS Biol 7:e1000089. CrossRef Medline

Benchenane K, Peyrache A, Khamassi M, Tierney PL, Gioanni Y, Battaglia FP, Wiener SI (2010) Coherent θ oscillations and reorganization of spike timing in the hippocampal-prefrontal network upon learning. Neuron 66:921–936. CrossRef Medline

Berens P (2009) CircStat: a MATLAB toolbox for circular statistic. J Stat Softw 31:1–21.

Bokil H, Andrews P, Kulkarni JE, Mehta S, Mitra PP (2010) Chronux: a platform for analyzing neural signals. J Neurosci Methods 192:146–151. CrossRef Medline

Bullock TH, Buzsáki G, McClune MC (1990) Coherence of compound field potentials reveals discontinuities in the CA1-subiculum of the hippocampus in freely-moving rats. Neuroscience 38:609–619. CrossRef Medline

Canolty RT, Edwards E, Dalal SS, Soltani M, Nagarajan SS, Kirsch HE, Berger MS, Barbaro NM, Knight RT (2006) High γ power is phase-locked to θ oscillations in human neocortex. Science 313:1626–1628. CrossRef Medline

DeCoteau WE, Thorn C, Gibson DJ, Courtemanche R, Mitra P, Kubota Y, Graybiel AM (2007) Learning-related coordination of striatal and hippocampal θ rhythms during acquisition of a procedural maze task. Proc Natl Acad Sci U S A 104:5644–5649. CrossRef Medline

Deshmukh SS, Yoganarasimha D, Voicu H, Knierim JJ (2010) θ modulation in the medial and lateral entorhinal cortices. J Neurophysiol 104:994–1006. CrossRef Medline

Dzirasa K, Ramsey AJ, Takahashi DY, Stapleton J, Potes JM, Williams JK, Gainetdinov RR, Sameshima K, Caron MG, Nicolelis MA (2009) Hyperdopaminergia and NMDA receptor hypofunction disrupt neural phase signaling. J Neurosci 29:8215–8224. CrossRef Medline

Fanselow MS, Dong HW (2010) Are the dorsal and ventral hippocampus functionally distinct structures? Neuron 65:7–19. CrossRef Medline

Fell J, Axmacher N (2011) The role of phase synchronization in memory processes. Nat Rev Neurosci 12:105–118. CrossRef Medline

Fellous JM, Sejnowski TJ (2000) Cholinergic induction of oscillations in the hippocampal slice in the slow (0.5–2 Hz), θ (5–12 Hz) and γ (35–70 Hz) bands. Hippocampus 10:187–197. CrossRef Medline

Fischer G, Mutel V, Trube G, Malherbe P, Kew JN, Mohacsi E, Heitz MP, Kemp JA (1997) Ro 25–6981, a highly potent and selective blocker of N-methyl-D-aspartate receptors containing the NR2B subunit. J Pharmacol Exp Ther 283:1285–1292. Medline

Fries P (2005) A mechanism for cognitive dynamics: neuronal communication through neuronal coherence. Trends Cogn Sci 9:474–480. CrossRef Medline

Fujisawa S, Buzsáki G (2011) A 4 Hz oscillation adaptively synchronizes prefrontal, VTA, and hippocampal activities. Neuron 72:153–165. CrossRef Medline

Giocomo LM, Zilli EA, Fransén E, Hasselmo ME (2007) Temporal frequency of subthreshold oscillations scales with entorhinal grid cell field spacing. Science 315:1719–1722. CrossRef Medline

Goutagny R, Jackson J, Williams S (2009) Self-generated θ oscillations in the hippocampus. Nat Neurosci 12:1491–1493. CrossRef Medline

Gu N, Jackson J, Goutagny R, Lowe G, Williams S (2011) The CA3 area contains distinct slow-θ oscillators at the dorsal and ventral regions in the complete hippocampus in vitro. Soc Neurosci Abstr 661.15/E6.

Hangya B, Borhegyi Z, Szilágyi N, Freund TF, Varga V (2009) GABAergic neurons of the medial septum lead the hippocampal network during θ activity. J Neurosci 29:8094–8102. CrossRef Medline

Hinman JR, Penley SC, Escabí MA, Chrobak JJ (2013) Ketamine disrupts θ synchrony across the septotemporal axis of the CA1 region of hippocampus. J Neurophysiol 109:570–579. CrossRef Medline

Hunt DL, Castillo PE (2012) Synaptic plasticity of NMDA receptors: mechanisms and functional implications. Curr Opin Neurobiol 22:496–508. CrossRef Medline

Isomura Y, Sirota A, Ozen S, Montgomery S, Mizuseki K, Henze DA, Buzsáki G (2006) Integration and segregation of activity in entorhinal–hip-

pocampal subregions by neocortical slow oscillations. Neuron 52:871–882. CrossRef Medline

Jackson J, Goutagny R, Williams S (2011) Fast and slow γ rhythms are intrinsically and independently generated in the subiculum. J Neurosci 31:12104–12117. CrossRef Medline

Kjelstrup KG, Tuvnes FA, Steffenach HA, Murison R, Moser EI, Moser MB (2002) Reduced fear expression after lesions of the ventral hippocampus. Proc Natl Acad Sci U S A 99:10825–10830. CrossRef Medline

Lachaux JP, Rodriguez E, Martinerie J, Varela FJ (1999) Measuring phase synchrony in brain signals. Hum Brain Mapp 8:194–208. CrossRef Medline

Le Van Quyen M, Bragin A (2007) Analysis of dynamic brain oscillations: methodological advances. Trends Neurosci 30:365–373. CrossRef Medline

Lee MG, Chrobak JJ, Sik A, Wiley RG, Buzsáki G (1994) Hippocampal θ activity following selective lesion of the septal cholinergic system. Neuroscience 62:1033–1047. CrossRef Medline

Lehner M, Wislowska-Stanek A, Skorzewska A, Maciejak P, Szyndler J, Turzynska D, Sobolewska A, Krzascik P, Plaznik A (2011) Expression of N-methyl-D-aspartate (R) (GluN2B) subunits in the brain structures of rats selected for low and high anxiety. J Physiol Pharmacol 62:473–482. Medline

Li XG, Somogyi P, Ylinen A, Buzsáki G (1994) The hippocampal CA3 network: an in vivo intracellular labeling study. J Comp Neurol 339:181–208. CrossRef Medline

Liu L, Wong TP, Pozza MF, Lingenhoehl K, Wang Y, Sheng M, Auberson YP, Wang YT (2004) Role of NMDA receptor subtypes in governing the direction of hippocampal synaptic plasticity. Science 304:1021–1024. CrossRef Medline

Marshall L, Born J (2007) The contribution of sleep to hippocampal-dependent memory consolidation. Trends Cogn Sci 11:442–450. CrossRef Medline

Melchers BP, Pennartz CM, Lopes da Silva FH (1987) Differential effects of elevated extracellular calcium concentrations on field potentials in dentate gyrus and CA1 of the rat hippocampal slice preparation. Neurosci Lett 77:37–42. CrossRef Medline

Mizuseki K, Sirota A, Pastalkova E, Buzsáki G (2009) θ oscillations provide temporal windows for local circuit computation in the entorhinal–hippocampal loop. Neuron 64:267–280. CrossRef Medline

Moser MB, Moser EI (1998) Functional differentiation in the hippocampus. Hippocampus 8:608–619. CrossRef Medline

Moser E, Moser MB, Andersen P (1993) Spatial learning impairment parallels the magnitude of dorsal hippocampal lesions, but is hardly present following ventral lesions. J Neurosci 13:3916–3925. Medline

Nakazawa K, Quirk MC, Chitwood RA, Watanabe M, Yeckel MF, Sun LD, Kato A, Carr CA, Johnston D, Wilson MA, Tonegawa S (2002) Requirement for hippocampal CA3 NMDA receptors in associative memory recall. Science 297:211–218. CrossRef Medline

Nascimento Häckl LP, Carobrez AP (2007) Distinct ventral and dorsal hippocampus AP5 anxiolytic effects revealed in the elevated plus-maze task in rats. Neurobiol Learn Mem 88:177–185. CrossRef Medline

Palva JM, Palva S, Kaila K (2005) Phase synchrony among neuronal oscillations in the human cortex. J Neurosci 25:3962–3972. CrossRef Medline

Papatheodoropoulos C, Moschovos C, Kostopoulos G (2005) Greater contribution of N-methyl-D-aspartic acid receptors in ventral compared to dorsal hippocampal slices in the expression and long-term maintenance of epileptiform activity. Neuroscience 135:765–779. CrossRef Medline

Patel J, Fujisawa S, Berényi A, Royer S, Buzsáki G (2012) Traveling θ waves along the entire septotemporal axis of the hippocampus. Neuron 75:410–417. CrossRef Medline

Pentkowski NS, Blanchard DC, Lever C, Litvin Y, Blanchard RJ (2006) Effects of lesions to the dorsal and ventral hippocampus on defensive behaviors in rats. Eur J Neurosci 23:2185–2196. CrossRef Medline

Popa D, Duvarci S, Popescu AT, Léna C, Paré D (2010) Coherent amygdalocortical θ promotes fear memory consolidation during paradoxical sleep. Proc Natl Acad Sci U S A 107:6516–6519. CrossRef Medline

Rebola N, Srikumar BN, Mulle C (2010) Activity-dependent synaptic plasticity of NMDA receptors. J Physiol 588:93–99. CrossRef Medline

Reymann KG, Matthies HK, Frey U, Vorobyev VS, Matthies H (1986) Calcium-induced long-term potentiation in the hippocampal slice: characterization of the time course and conditions. Brain Res Bull 17:291–296. CrossRef Medline

Rodriguez E, George N, Lachaux JP, Martinerie J, Renault B, Varela FJ (1999) Perception's shadow: long-distance synchronization of human brain activity. Nature 397:430–433. CrossRef Medline

Royer S, Sirota A, Patel J, Buzsáki G (2010) Distinct representations and θ dynamics in dorsal and ventral hippocampus. J Neurosci 30:1777–1787. CrossRef Medline

Sabolek HR, Penley SC, Hinman JR, Bunce JG, Markus EJ, Escabi M, Chrobak JJ (2009) θ and γ coherence along the septotemporal axis of the hippocampus. J Neurophysiol 101:1192–1200. CrossRef Medline

Scimemi A, Fine A, Kullmann DM, Rusakov DA (2004) NR2B-containing receptors mediate cross talk among hippocampal synapses. J Neurosci 24:4767–4777. CrossRef Medline

Seidenbecher T, Laxmi TR, Stork O, Pape HC (2003) Amygdalar and hippocampal θ rhythm synchronization during fear memory retrieval. Science 301:846–850. CrossRef Medline

Siapas AG, Lubenov EV, Wilson MA (2005) Prefrontal phase locking to hippocampal θ oscillations. Neuron 46:141–151. CrossRef Medline

Sigurdsson T, Stark KL, Karayiorgou M, Gogos JA, Gordon JA (2010) Impaired hippocampal–prefrontal synchrony in a genetic mouse model of schizophrenia. Nature 464:763–767. CrossRef Medline

Steffenach HA, Sloviter RS, Moser EI, Moser MB (2002) Impaired retention of spatial memory after transection of longitudinally oriented axons of hippocampal CA3 pyramidal cells. Proc Natl Acad Sci U S A 99:3194–3198. CrossRef Medline

Stocca G, Vicini S (1998) Increased contribution of NR2A subunit to synaptic NMDA receptors in developing rat cortical neurons. J Physiol 507:13–24. CrossRef Medline

Swanson LW, Cowan WM (1977) An autoradiographic study of the organization of the efferent connections of the hippocampal formation in the rat. J Comp Neurol 172:49–84. CrossRef Medline

Takehara-Nishiuchi K, Maal-Bared G, Morrissey MD (2011) Increased entorhinal–prefrontal θ synchronization parallels decreased entorhinal–hippocampal θ synchronization during learning and consolidation of associative memory. Front Behav Neurosci 5:90. CrossRef Medline

Tang YP, Shimizu E, Dube GR, Rampon C, Kerchner GA, Zhuo M, Liu G, Tsien JZ (1999) Genetic enhancement of learning and memory in mice. Nature 401:63–69. CrossRef Medline

Tort AB, Komorowski R, Eichenbaum H, Kopell N (2010) Measuring phase-amplitude coupling between neuronal oscillations of different frequencies. J Neurophysiol 104:1195–1210. CrossRef Medline

Tovar KR, Westbrook GL (1999) The incorporation of NMDA receptors with a distinct subunit composition at nascent hippocampal synapses in vitro. J Neurosci 19:4180–4188. Medline

Turner RW, Baimbridge KG, Miller JJ (1982) Calcium-induced long-term potentiation in the hippocampus. Neuroscience 7:1411–1416. CrossRef Medline

Watrous AJ, Tandon N, Conner CR, Pieters T, Ekstrom AD (2013) Frequency-specific network connectivity increases underlie accurate spatiotemporal memory retrieval. Nat Neurosci 16:349–356. CrossRef Medline

Wolansky T, Clement EA, Peters SR, Palczak MA, Dickson CT (2006) Hippocampal slow oscillation: a novel EEG state and its coordination with ongoing neocortical activity. J Neurosci 26:6213–6229. CrossRef Medline

Womelsdorf T, Schoffelen JM, Oostenveld R, Singer W, Desimone R, Engel AK, Fries P (2007) Modulation of neuronal interactions through neuronal synchronization. Science 316:1609–1612. CrossRef Medline

Wu CP, Huang HL, Asl MN, He JW, Gillis J, Skinner FK, Zhang L (2006) Spontaneous rhythmic field potentials of isolated mouse hippocampal-subicular-entorhinal cortices in vitro. J Physiol 576:457–476. CrossRef Medline